Ovariectomy induces bone loss via microbial-dependent trafficking of intestinal TNF$^+$ T cells and Th17 cells

Mingcan Yu,[1,2] Subhashis Pal,[1,2] Cameron W. Paterson,[3,4] Jau-Yi Li,[1,2] Abdul Malik Tyagi,[1,2] Jonathan Adams,[1,2] Craig M. Coopersmith,[2,3] M. Neale Weitzmann,[1,2,5] and Roberto Pacifici[1,2,6]

[1]Division of Endocrinology, Metabolism and Lipids, Department of Medicine and [2]Emory Microbiome Research Center, Emory University, Atlanta, Georgia, USA. [3]Department of Surgery and Emory Critical Care Center, Emory University School of Medicine, Atlanta, Georgia, USA. [4]Medical Corps, United States Navy, NROTC, Atlanta, Georgia, USA. [5]Atlanta VA Medical Center, Decatur, Georgia, USA. [6]Immunology and Molecular Pathogenesis Program, Emory University, Atlanta, Georgia, USA.

Estrogen deficiency causes a gut microbiome–dependent expansion of BM Th17 cells and TNF-α–producing T cells. The resulting increased BM levels of IL-17a (IL-17) and TNF stimulate RANKL expression and activity, causing bone loss. However, the origin of BM Th17 cells and TNF$^+$ T cells is unknown. Here, we show that ovariectomy (ovx) expanded intestinal Th17 cells and TNF$^+$ T cells, increased their S1P receptor 1–mediated (S1PR1-mediated) egress from the intestine, and enhanced their subsequent influx into the BM through CXCR3- and CCL20-mediated mechanisms. Demonstrating the functional relevance of T cell trafficking, blockade of Th17 cell and TNF$^+$ T cell egress from the gut or their influx into the BM prevented ovx-induced bone loss. Therefore, intestinal T cells are a proximal target of sex steroid deficiency relevant for bone loss. Blockade of intestinal T cell migration may represent a therapeutic strategy for the treatment of postmenopausal bone loss.

Introduction

Postmenopausal osteoporosis is a common skeletal disease that leads to bone fractures and disability. The disease stems mainly from the cessation of ovarian function, in which declining estrogen levels result in the stimulation of bone resorption and, to a lesser extent, bone formation, driving a period of rapid bone loss (1). In mice, the effects of estrogen depletion are modeled by ovariectomy (ovx). At the cellular level, the central mechanisms by which estrogen deficiency induces bone loss are increased osteoclast formation (1, 2) and osteoclast life span (3, 4). The primary drivers of increased osteoclastogenesis are enhanced production of the immune factors RANKL, TNF, and IL-17 and decreased secretion of the RANKL antagonist osteoprotegerin (OPG) (1, 5). While RANKL is the ultimate inducer of osteoclast formation, TNF potentiates RANKL activity (6, 7) and induces the expansion of Th17 cells (8–10). Th17 cells are an osteoclastogenic population of CD4$^+$ cells (11, 12) defined by the capacity to produce IL-17 (13). Th17 cells potently induce osteoclastogenesis by secreting IL-17, RANKL, and TNF along with low levels of IFN-γ (14–16). IL-17 stimulates the release of RANKL by all osteoblastic cells, including osteocytes (8, 17), and increases the osteoclastogenic activity of RANKL by upregulating RANK (18). In addition, IL-17 blunts bone formation (19, 20).

Many cell types express RANKL, including osteoblasts, osteocytes, T cells, and B cells (21–23). Osteocytes are among the most relevant sources of RANKL in estrogen-deficient mice (23). In humans, estrogen deficiency is associated with an expansion of T cells expressing RANKL, TNF, and IL-17 (21, 22, 24–26). The contributing influences of RANKL, IL-17, and TNF in humans are underscored by reports showing that menopause increases the levels of these immune factors (21, 26–28), while treatment with TNF inhibitors prevents the increase in bone resorption that results from estrogen deficiency (29). In the mouse, the causal role of T cells and TNF in ovx-induced bone loss has been demonstrated in multiple models (30–32). For example, ovx- induced bone loss did not occur in mice lacking T cell TNF production (6, 30, 33, 34) or lacking the costimulatory molecule CD40L (35) as well as mice treated with CTLA4-Ig, an agent that transmits an inhibitory signal to T cells (36).

The relevance of Th17 cells and IL-17 for the bone loss induced by ovx in mice is demonstrated by the expansion of BM Th17 cells and increased production of IL-17 in response to ovx (37, 38) and by reports that treatment with anti–IL-17 Ab or silencing of IL-17 signaling prevent ovx-induced bone loss (39–41). Th17 cells and IL-17 have also been implicated in the bone loss induced by inflammation (12, 42) and parathyroid hormone (PTH) (8, 43).

In the mouse, Th17 cells are mostly produced and reside in the intestinal lamina propria, where their development depends on the presence of segmented filamentous bacteria (SFB) (44), which are spore-forming, Gram-positive commensal bacteria that potently induce differentiation of Th17 cells (45, 46). In humans, about 20 nonvirulent gut bacterial strains are known to induce Th17 cell differentiation (47, 48).

We reported that germ-free mice are protected against the bone loss induced by sex steroid deprivation (38), a find-

Authorship note: MY and SP are co–first authors.
Conflict of interest: The authors have declared that no conflict of interest exists.

Submitted: August 10, 2020; **Accepted:** December 1, 2020; **Published:** February 15, 2021.
Reference information: *J Clin Invest*. 2021;131(4):e143137.
https://doi.org/10.1172/JCI143137.

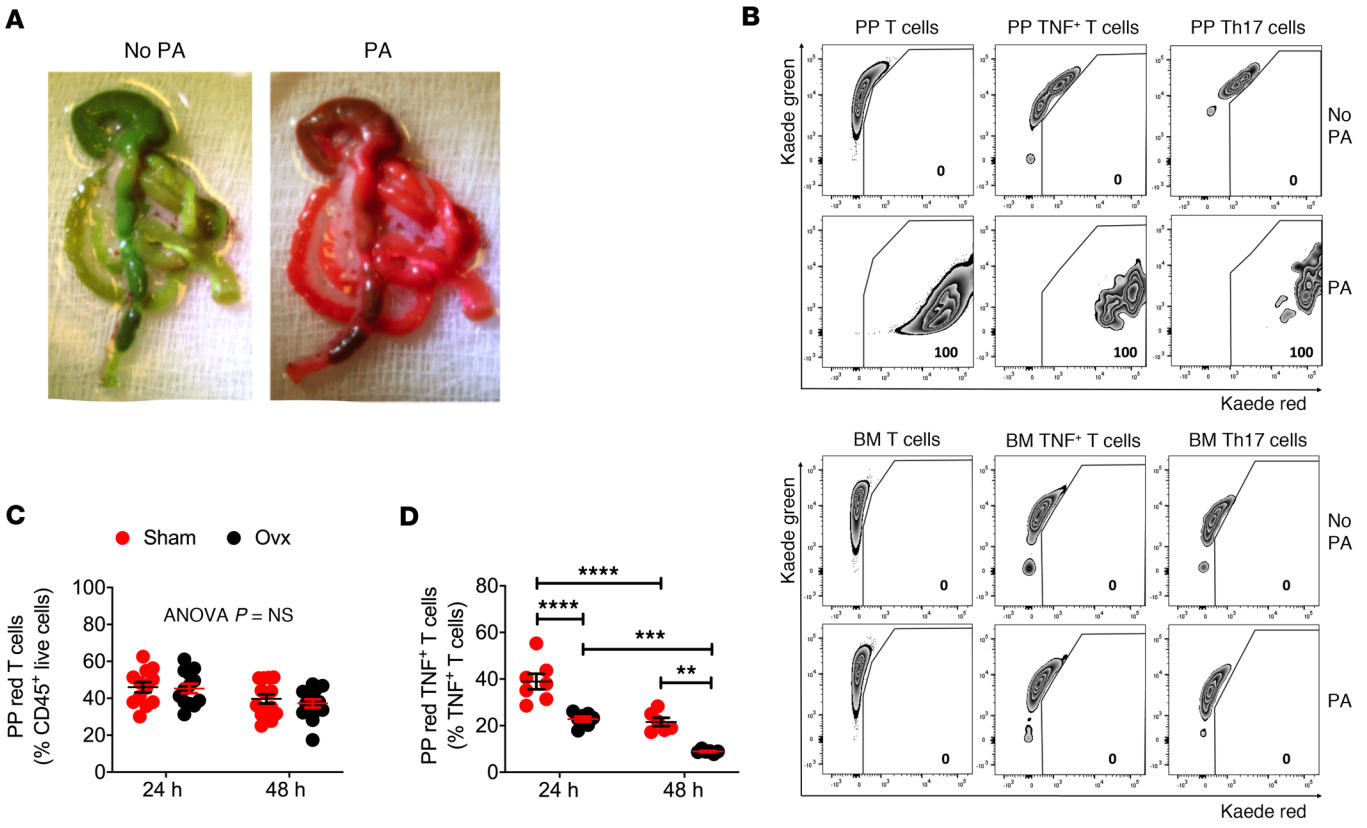

J Clin Invest. 2021;131(4):e143137 https://doi.org/10.1172/JCI143137

Figure 1. Ovx increases the trafficking of T cells from the gut to the BM. (**A**) Image of the intestine of Kaede mice before and after ex vivo photoconversion of the dissected organ by exposure to a 390 nm wavelength light for 2 minutes. (**B**) Representative flow cytometric analysis of T cells harvested from photoactivated (PA) PPs and BM of Kaede mice subjected or not subjected to in vivo photoconversion. Plots show the relative frequency of KaedeR total T cells, TNF$^+$ T cells, and Th17 cells. Ten-week-old female SFB$^+$ Kaede mice were subjected to surgical laparotomy to access the PPs in the distal SI. PP cells were photoconverted by exposing them to a 390 nm light for 2 minutes. Mice were sacrificed immediately after the photoconversion. (**C**–**E**) Relative frequency of KaedeR total T cells, TNF$^+$ T cells, and Th17 cells in PPs from sham-operated mice and mice that had undergone ovx 24 hours and 48 hours after photoconversion. (**F** and **G**) Relative and absolute frequency of KaedeR total T cells in the BM of sham-operated mice and mice that had undergone ovx 24 hours and 48 hours after photoconversion. (**H** and **I**) Relative and absolute frequency of KaedeR total TNF$^+$ T cells in the BM of sham-operated mice and mice that had undergone ovx 24 hours and 48 hours after photoconversion. (**J** and **K**) Relative and absolute frequency of KaedeR total Th17 cells in the BM of sham-operated mice and mice that had undergone ovx 24 hours and 48 hours after photoconversion. For panels **C**–**K**, 10-week-old Kaede mice were subjected to either ovx or sham surgery. After 2 weeks, mice underwent surgical laparotomy and PP cells were photoconverted. Mice were sacrificed 24 or 48 hours later and the number of KaedeR T cells in PPs and BM measured by flow cytometry. n = 6–14 mice per group. Data are expressed as mean ± SEM. All data were normally distributed according to the Shapiro-Wilk normality test and analyzed by 2-way ANOVA and post hoc tests applying Bonferroni's correction for multiple comparisons. $^*P < 0.05$; $^{**}P < 0.01$; $^{***}P < 0.001$; $^{****}P < 0.0001$, compared with the indicated group.

ing suggesting the gut microbiome to be the source of antigens driving T cell activation in mice that had undergone ovx. We further reported that sex steroid deficiency increases gut permeability, allowing microbial components to activate T cells and expand TNF$^+$ T cells and Th17 cells in the intestinal wall, thus increasing the production of TNF and IL-17 in the lamina propria of the intestinal wall (38). A link among menopause, gut permeability, inflammation, and bone loss has recently been confirmed in humans (49). The expansion of intestinal T cells and the increase in their production of osteoclastogenic cytokines production induced by sex steroid deprivation mirrored similar changes in T cell number and cytokine levels in the BM (38). This suggests that T cells first become activated and expand in the gut in response to microbial stimuli and then migrate from the gut to the BM, leading to an expansion of BM T cells, enhanced cytokine production, and bone loss. However, whether BM T cells implicated in bone loss originate in the gut remains unknown.

In this study, we investigated the effects of ovx on the trafficking of T cells from the gut to the BM. We show that ovx increases the egress of TNF$^+$ T cells and Th17 cells from the gut to the systemic circulation and their subsequent influx into the BM. Moreover, we show that blockade of T cell egress from the gut or influx into the BM prevents the expansion of BM T cells induced by ovx and prevents ovx-induced bone loss.

Results

Ovx increases the trafficking of T cells from the small intestine to the BM. Ovx increases gut permeability, causing translocation of bacterial products such as LPS and flagellin that increase activation of T cells in the lamina propria of the intestinal wall (38). Since intestinal T cells have the capacity to migrate to distant organs driven by chemokine gradients (50, 51), ovx may cause the homing of intestinal T cells to the BM. To directly investigate the effect of ovx on T cell trafficking, we made use of C57BL/6 Kaede mice (52). This strain offers a sensitive means for tracking the migration from the gut to anatomically distant sites of any leukocyte cell type definable by surface-displayed or intracellular markers. Kaede mice ubiquitously express the photoconvertible protein Kaede, which permanently changes their fluorescence emission from green (518 nm) to red (582 nm) upon photoactivation with near-UV light (350-410 nm). Once photoconverted in the intestine, red fluorescing cells can be detected and enumerated by flow cytometry in other organs. The photoconversion of intracellular Kaede has no effect on cellular function and on the homing capacity of T cells (53). Hereafter, we will refer to photoconverted cells as KaedeR cells. The original colony of Kaede mice established in our vivarium were SFB$^-$. To utilize a model in which Th17 cells can expand in the gut, we generated SFB$^+$ Kaede mice by gavaging the mice with a liquid suspension of stools from mice previously monocolonized with SFB (43). Figure 1A shows the intestine of a Kaede mouse before and after photoactivation of the dissected organ ex vivo by exposure to a 390 nm light for 2 minutes.

To assess the efficiency of the photoconversion in vivo, 10-week-old female SFB$^+$ Kaede mice were subjected to surgical laparotomy to access Peyer's patches (PP) in the distal small intestine (SI). Three to four PPs/mouse were photoconverted by exposing them to a 390 nm light for 2 minutes. To make sure that no other cells were photoconverted, the whole mouse was covered with an aluminum foil blanket. Mice were sacrificed immediately after the photoconversion, and the relative frequencies of KaedeR total T cells, TNF$^+$ T cells, and Th17 cells in the PPs subjected to photoconversion and in the BM were measured by flow cytometry. This analysis revealed that more than 98% of T cells from PPs exposed to near-UV light underwent photoconversion, whereas KaedeR cells were undetectable in the BM (Figure 1B). Confirming that photoactivation of PPs does not photoconvert bone tissue and BM cells, femurs and tibiae harvested from Kaede mice immediately after PP photoactivation were of a similar green color (Supplemental Figure 1A; supplemental material available online with this article; https://doi.org/10.1172/JCI143137DS1). Moreover, analysis of BM cells by fluorescence microscopy did not reveal the presence of red fluorescing cells in the BM of Kaede mice immediately after PP photoactivation (Supplemental Figure 1, B and C).

Next, 10-week-old SFB$^+$ Kaede mice were subjected to either ovx or sham surgery. Two weeks later, all animals were subjected to surgical laparotomy and 3 to 4 PPs/mouse were photoactivated. Mice were sacrificed 24 or 48 hours later and the number of KaedeR T cells in PPs and BM measured by flow cytometry. Because the measurement of the absolute number of PP cells is technically challenging due to variability of the size of the collected PP tissue, PP KaedeR cells were quantified only as percentages of total cells. Analysis of the cells harvested from the photoactivated PPs revealed that sham-operated mice and mice that had undergone ovx had a similar relative frequency of PP KaedeR total T cells 24 to 48 hours after photoactivation (Figure 1C and Supplemental

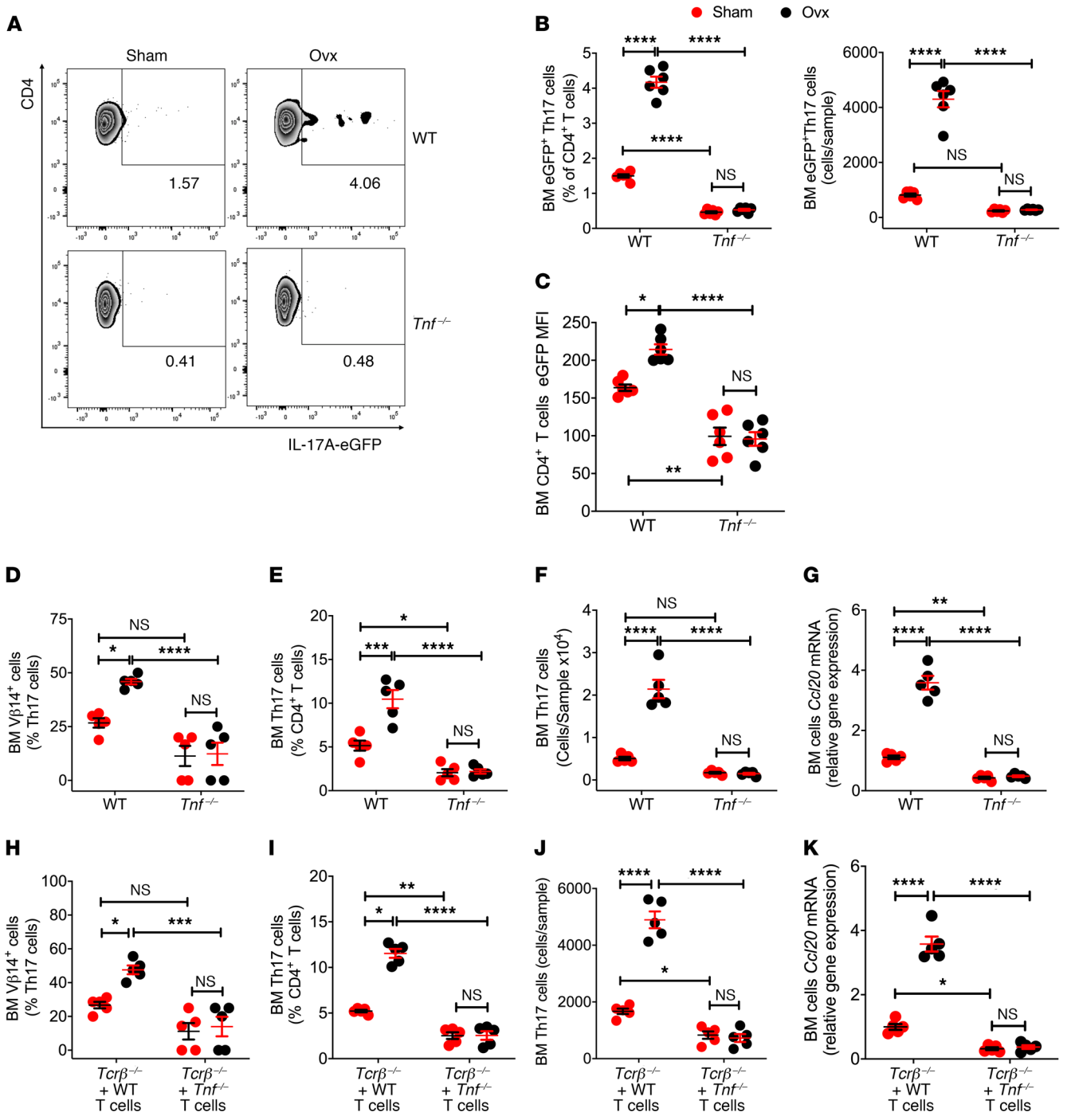

Figure 2. Ovx increases the trophism of BM Th17 cells for the BM via a TNF-dependent mechanism. (**A**) Representative flow cytometry plot and frequency of EGFP⁺ Th17 cells in the BM of WT and *Tnf*$^{-/-}$ sham-operated mice and mice that had undergone ovx. (**B**) Relative and absolute frequency of EGFP⁺ Th17 cells in the BM of WT and *Tnf*$^{-/-}$ mice subjected to sham surgery or ovx 2 weeks before adoptive transfer of IL-17A-EGFP⁺ cells. (**C**) BM CD4⁺ T cell EGFP MFI. In these experiments, EGFP⁺CD4⁺ Th17 cells were injected i.v. into WT and *Tnf*$^{-/-}$ mice that had been subjected to sham operation or ovx 14 days before the T cell transfer. Twenty-four hours after transfer, EGFP⁺CD4⁺ T cells (EGFP⁺ Th17 cells) were enumerated by flow cytometry in BM of recipient mice. (**D**) Relative frequency of BM Vβ14⁺ Th17 cells in WT and *Tnf*$^{-/-}$ mice. (**E** and **F**) Relative and absolute frequency of BM of total Th17 cells in WT and *Tnf*$^{-/-}$ mice. (**G**) BM *Ccl20* transcript levels in *Tnf*$^{-/-}$ mice. (**H**) Relative frequency of BM Vβ14⁺ Th17 cells in *Tcrβ*$^{-/-}$ mice reconstituted with WT T cells or *Tnf*$^{-/-}$ T cells. (**I** and **J**) Relative and absolute frequency of BM of total Th17 cells in *Tcrβ*$^{-/-}$ mice reconstituted with WT T cells or *Tnf*$^{-/-}$ T cells. (**K**) BM *Ccl20* transcript levels in *Tcrβ*$^{-/-}$ mice reconstituted with WT T cells or *Tnf*$^{-/-}$ T cells. n = 5–6 mice per group. Data are expressed as mean ± SEM. All data were normally distributed according to the Shapiro-Wilk normality test and analyzed by 2-way ANOVA and post hoc tests applying Bonferroni's correction for multiple comparisons. *P < 0.05; **P < 0.01; ***P < 0.001; ****P < 0.0001, compared with the indicated group.

Figure 2A). Analysis of KaedeR T cell subpopulations revealed that ovx decreased the relative frequency of PP KaedeR TNF$^+$ T cells and PP KaedeR Th17 cells at 24 and 48 hours (Figure 1, D and E, and Supplemental Figure 2, B and C), indicating that ovx increases the egress of TNF$^+$ T cells and Th17 cells from PPs. Analysis of BM cells from sham-operated mice revealed that less than 0.5% of the BM hematopoietic cells (CD45$^+$ cells) were KaedeR T cells (Figure 1F). This was consistent with the fact that, having photoconverted only the cells of 3 to 4 PPs/mouse, most of the intestinal T cells with the potential to migrate to the BM were Kaede green cells. However, ovx markedly increased the relative and absolute frequency of BM KaedeR total T cells at 24 and 48 hours (Figure 1, F and G). Moreover, ovx increased the relative and absolute frequency of BM KaedeR TNF$^+$ T cells and Th17 cells at 24 hours, while it increased the absolute but not the relative number of TNF$^+$ T cells and Th17 cells at 48 hours (Figure 1, H–K). Together, these data demonstrate that ovx promotes the migration of intestinal total T cells, TNF$^+$ T cells, and Th17 cells from intestinal tissues to the BM. The finding of an absolute but not relative increase in KaedeR TNF$^+$ T cells and Th17 cells at 48 hours may further suggest that additional populations of cells may accumulate in the BM at 48 hours.

To investigate the hypothesis that an influx of TNF$^+$ T cells in the BM and the resulting increased production of TNF are required for the homing of Th17 cells to the BM, we conducted experiments using *Il17a* EGFP mice and *Tnf*$^{-/-}$ mice. *Il17a* EGFP reporter mice possess an IRES-EGFP sequence after the stop codon of the *Il17a* gene, so that EGFP expression is limited to IL-17A–expressing cells, thus allowing Th17 cells to be detected by measuring EGFP by flow cytometry. Splenic naive CD4$^+$ cells (CD4$^+$CD44^{lo}CD62L^{hi} cells), which are EGFP$^-$, were purified from *Il17a* EGFP mice and cultured in Th17 cell–polarizing conditions for 4 days. Th17 cells (CD4$^+$EGFP$^+$ cells) were then FACS sorted and transferred into WT and *Tnf*$^{-/-}$ mice that had been subjected to sham operation or ovx 2 weeks earlier. One day after T cell transfer, the recipient mice were sacrificed and BM Th17 cells (CD4$^+$EGFP$^+$ cells) enumerated by flow cytometry. WT mice that had undergone ovx had a higher relative and absolute number of EGFP$^+$ Th17 cells in the BM than WT sham-operated controls. In contrast, ovx did not increase the frequency of BM EGFP$^+$ Th17 cells in *Tnf*$^{-/-}$ mice (Figure 2, A and B). In addition, ovx increased the EGFP mean fluorescence intensity of CD4$^+$ T cells in WT, but not in *Tnf*$^{-/-}$, mice (Figure 2C). These findings demonstrated that ovx increases the recruitment of Th17 cells to the BM via a TNF-dependent mechanism.

In mice, most of the Th17 cells produced in the lamina propria of the intestinal wall contain the Vβ14 chain in their TCR receptors (54, 55). Accordingly, we found that ovx upregulated the frequency of BM Vβ14$^+$ Th17 cells as well as the relative and absolute frequency of the overall population of Th17 cells in WT mice but not in *Tnf*$^{-/-}$ mice (Figure 2, D–F). These findings provide further support to the hypothesis that ovx increases the migration of Th17 cells from the gut to the BM via a TNF-dependent mechanism.

The homing of Th17 cells to the BM is driven by the chemokine ligand CCL20, which is expressed by BM stromal cells (43), and by the chemokine receptor CCR6, which is expressed by Th17 cells (56). CCL20 is strongly induced by inflammatory cytokines, including TNF (50). This suggests that the expansion of the BM pool of TNF$^+$ T cells induced by ovx and the resulting increase in the BM levels of TNF may upregulate CCL20 expression by BM cells, causing the chemotactic migration of Th17 cells from the gut to the BM. In support of this hypothesis, we found that ovx upregulated BM *Ccl20* transcripts in WT mice but not in *Tnf*$^{-/-}$ mice (Figure 2G).

To investigate the specific role of the pool of TNF produced by T cells, splenic T cells from WT and *Tnf*$^{-/-}$ mice were transferred into *Tcrβ*$^{-/-}$ mice, a strain lacking αβ T cells. After 2 weeks, a length of time sufficient for the engraftment and expansion of donor T cells, recipient mice were subjected to sham operation or ovx and sacrificed 2 weeks after surgery. Ovx upregulated the frequency of BM Vβ14$^+$ Th17 cells, and the relative and absolute frequency of total Th17 cells in mice with WT T cells, but not in those with *Tnf*$^{-/-}$ T cells (Figure 2, H–J). Moreover, ovx increased expression of *Ccl20* in the BM of host mice with WT T cells, but not in those with *Tnf*$^{-/-}$ T cells (Figure 2K). These findings demonstrate that the production of TNF by T cells is required for ovx to expand Th17 cells and upregulate CCL20 expression by BM cells.

S1PR1 induces T cell egress from the SI. T cells express S1P receptor 1 (S1PR1), which promotes lymphocyte egress from intestinal lymphoid tissues in response to sensing of circulating S1P (57). This suggests that ovx may promote the egress of TNF$^+$ T cells and Th17 cells from the intestine through a S1PR1-mediated mechanism. To determine whether ovx promotes the exit of PP TNF$^+$ T cells and Th17 from the intestine and does so via S1PR1, SFB$^+$ mice received ovx and were treated for 4 weeks with the S1PR1 functional antagonist FTY720, which is an agent that arrests lymphocyte exit from PPs and mesenteric lymph nodes without affecting lymphocyte function (58, 59). FTY720 did not block the increase in PP TNF$^+$ T cells induced by ovx, but it prevented the increase in BM TNF$^+$ T cells and BM *Tnf* transcript levels induced by ovx (Figure 3A). Similarly, FTY720 did not alter the capacity of ovx to increase PP Th17 cells, but it blocked the increase in the BM of Th17 cells, Vβ14$^+$ Th17 cells, and *Il17a* transcript levels induced by ovx (Figure 3B). Together, these findings showed that the egress of TNF$^+$ T cells and Th17 cells from the gut and their homing to the BM is mediated by S1PR1 signaling.

Attesting to the functional relevance of these effects, measurement of indices of trabecular bone volume and structure by in vitro μCT scanning at 4 weeks after ovx revealed that FTY720 completely prevented the loss of femoral and vertebral trabecular volume/total volume fraction (BV/TV), and the changes in trabecular thickness (Tb.Th), trabecular number (Tb.N), and trabecular separation (Tb.Sp) induced by ovx (Figure 3, C and D). In addition, FTY720 prevented the ovx-induced increase in serum C-terminal telopeptide of collagen type I (CTX), a marker of bone resorption, and serum osteocalcin, a marker of bone formation (Figure 3E). In contrast, FTY720 did not decrease the loss of femoral cortical area (Ct.Ar) and cortical thickness (Ct.Th) induced by ovx (Figure 3F), indicating that ovx caused cortical bone loss with mechanisms unrelated to T cell trafficking.

CCL20 and CXCR3 guide the influx T cell into the BM. Following their exit from the intestine, Th17 cells migrate to sites of inflammation guided by the CCR6/CCL20 axis (60). To determine the role of CCL20-driven influx of Th17 cells into the BM for the mechanism of action of ovx in bone, SFB$^+$ mice underwent ovx or sham operation and were treated with a neutralizing anti-CCL20

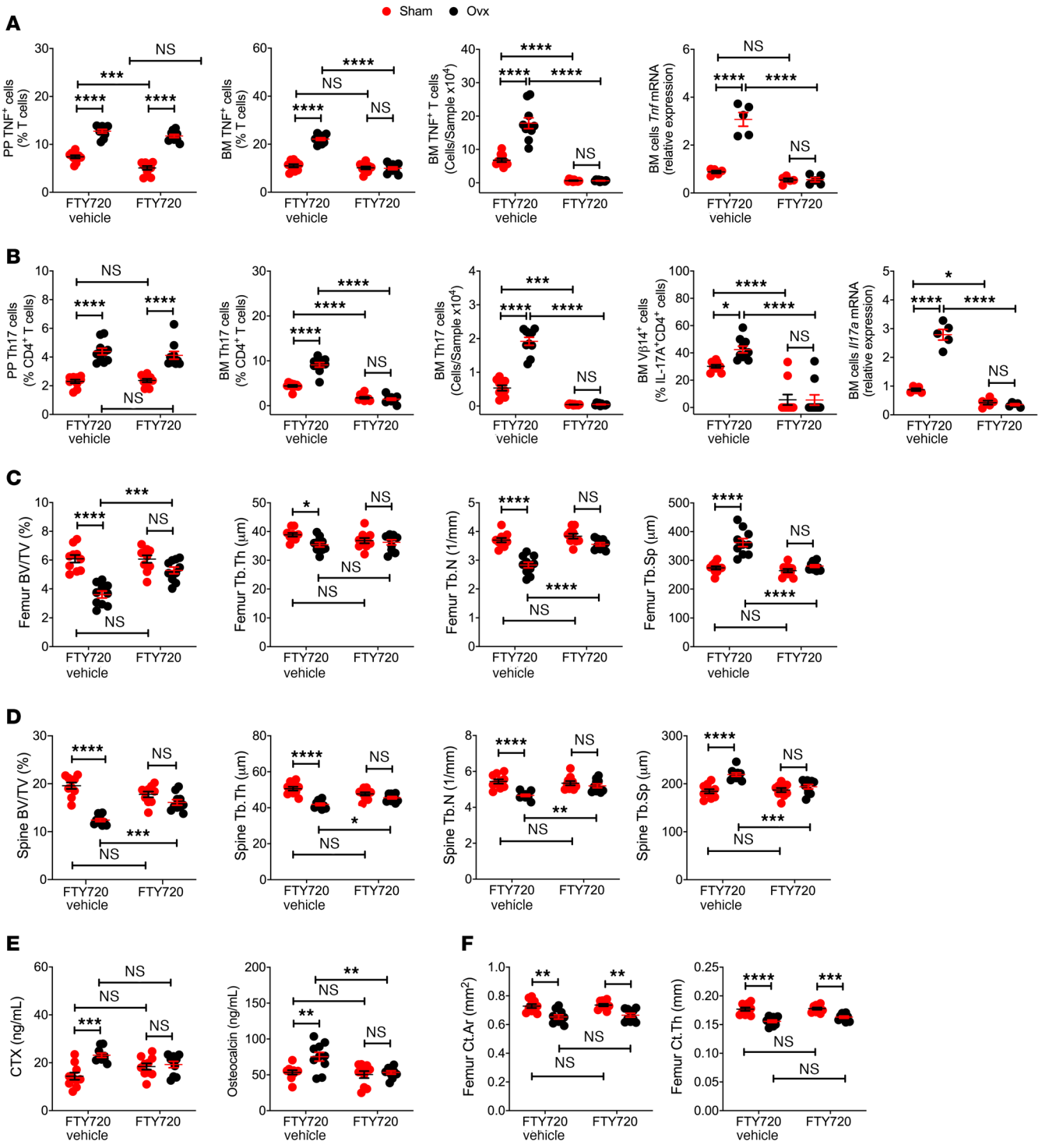

Figure 3. Blockade of T cell egress from the intestine prevents the expansion of TNF⁺ T cells and Th17 cells and bone loss induced by ovx. (**A**) Effects of ovx on the number of PP and BM TNF⁺ T cells and on the level of *Tnf* transcripts in mice treated with FTY720. (**B**) Effects of ovx on the number of PP and BM Th17 cells and on the level of *Il17a* transcripts in mice treated with FTY720. (**C**) Effects of ovx on BV/TV, Tb.Th, Tb.N, and Tb.Sp in mice treated with FTY720. (**D**) Effects of ovx on spinal BV/TV, Tb.Th, Tb.N, and Tb.Sp in mice treated with FTY720. (**E**) Effects of ovx on serum CTX levels and serum osteocalcin levels in mice treated with FTY720. (**F**) Effects of ovx on femoral Ct.Ar and Ct.Th in mice treated with FTY720. $n = 10$ mice per group. Data are expressed as mean ± SEM. All data were normally distributed according to the Shapiro-Wilk normality test and analyzed by 2-way ANOVA and post hoc tests applying Bonferroni's correction for multiple comparisons. $^*P < 0.05$; $^{**}P < 0.01$; $^{***}P < 0.001$; $^{****}P < 0.0001$, compared with the indicated group.

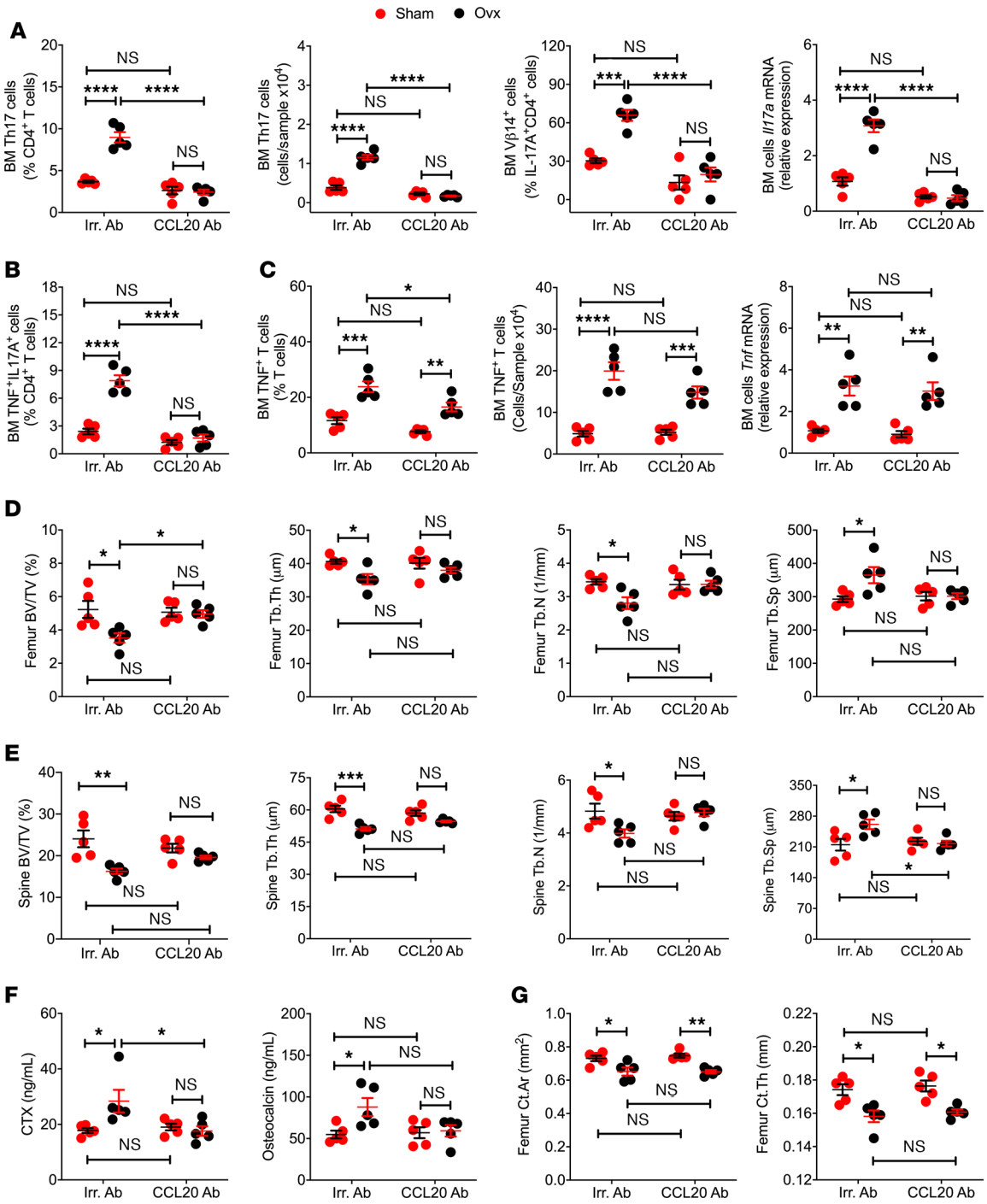

Figure 4. Blockade of Th17 cell influx into BM by treatment with anti-CCL20 Ab prevents expansion of Th17 cells and bone loss induced by ovx. (**A**) Effects of ovx on the frequency of BM Th17 cells and Vβ14$^+$ Th17 cells and on the level of *Il17a* transcripts. (**B**) Effects of ovx on the frequency of BM TNF$^+$IL-17$^+$ T cells. (**C**) Effects of ovx on the number of BM TNF$^+$ T cells and on the level of *Tnf* transcripts. (**D**) Effects of ovx on femoral BV/TV, Tb.Th, Tb.N, and Tb.Sp. (**E**) Effects of ovx on spinal BV/TV, Tb.Th, Tb.N, and Tb.Sp. (**F**) Effects of ovx on serum CTX levels and serum osteocalcin levels. (**G**) Effects of ovx on femoral Ct.Ar and Ct.Th. Mice were treated with anti-CCL20 Ab or irrelevant (Irr.) Ab. $n = 5$ mice per group. Data are expressed as mean ± SEM. All data were normally distributed according to the Shapiro-Wilk normality test and analyzed by 2-way ANOVA and post hoc tests applying Bonferroni's correction for multiple comparisons. *$P < 0.05$; **$P < 0.01$; ***$P < 0.001$; ****$P < 0.0001$, compared with the indicated group.

Ab or isotype-matched irrelevant Ab for 4 weeks. CCL20 Ab completely prevented the increase in BM Th17 cells, Vβ14$^+$ Th17 cells, and *Il17a* transcript levels induced by ovx (Figure 4A). Since Th17 cells are known to produce TNF, in this experiment, we also determined the fraction of TNF$^+$IL-17$^+$ cells and found that anti-CCL20 Ab prevented the increase in this subset of Th17 cells induced by ovx (Figure 4B). In contrast, CCL20 Ab did not block the increase in BM TNF$^+$ T cells and BM *Tnf* transcript levels induced by ovx (Figure 4C), indicating that CCL20 does not contribute to regulating the influx of TNF$^+$ T cells into the BM.

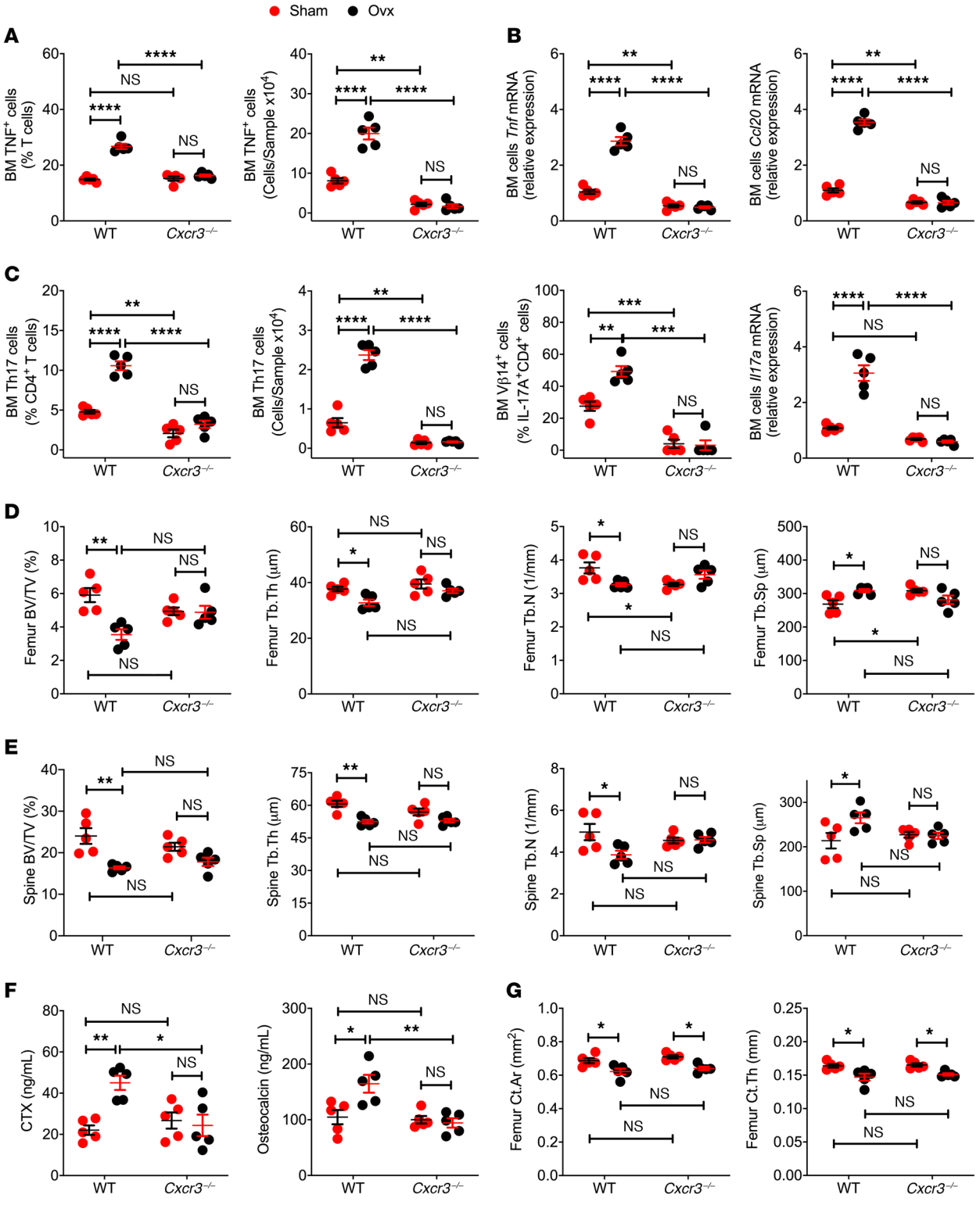

Figure 5. Blockade of T cell influx into BM by silencing of CXCR3 prevents expansion of TNF⁺ T cells and Th17 cells and bone loss induced by ovx. (**A**) Effects of ovx on the number of BM TNF⁺ T cells and on the level of *Tnf* transcripts in WT mice and *Cxcr3*$^{-/-}$ mice. (**B**) Effects of ovx on the BM cell transcript levels of *Ccl20* in WT mice and *Cxcr3*$^{-/-}$ mice. (**C**) Effects of ovx on the number of BM Th17 cells and on the levels of *Il17a* transcripts in WT mice and *Cxcr3*$^{-/-}$ mice. (**D**) Effects of ovx on femoral BV/TV, Tb.Th, Tb.N, and Tb.Sp in WT mice and *Cxcr3*$^{-/-}$ mice. (**E**) Effects of ovx on spinal BV/TV, Tb.Th, Tb.N, and Tb.Sp in WT mice and *Cxcr3*$^{-/-}$ mice. (**F**) Effects of ovx on serum CTX levels and serum osteocalcin levels in WT mice and *Cxcr3*$^{-/-}$ mice. (**G**) Effects of ovx on femoral Ct.Ar and Ct.Th in WT mice and *Cxcr3*$^{-/-}$ mice. $n = 5$ mice per group. Data are expressed as mean ± SEM. All data were normally distributed according to the Shapiro-Wilk normality test and analyzed by 2-way ANOVA and post hoc tests applying Bonferroni's correction for multiple comparisons. *$P < 0.05$; **$P < 0.01$; ***$P < 0.001$; ****$P < 0.0001$, compared with the indicated group.

Supporting evidence for an essential function of CCL20 and the migration of Th17 cells to the BM, treatment with anti-CCL20 Ab for 4 weeks prevented the loss of BV/TV, Tb.Th, and Tb.N and the increase in Tb.Sp in the femur and the lumbar spine, as measured by in vitro μCT scanning (Figure 4, D and E). Treatment with CCL20 Ab prevented the increased serum CTX and osteocalcin induced by ovx (Figure 4F), indicating that homing of Th17 cells to the BM contributes to the acceleration of bone turnover induced by ovx. In contrast, anti-CCL20 Abs did not decrease the loss of Ct.Ar and Ct.Th induced by ovx (Figure 4G), indicating that ovx caused cortical bone loss with mechanisms unrelated to Th17 cell trafficking.

While the egress of T cells from intestinal lymphoid tissues and their entrance into the bloodstream is driven by S1P/S1PR1 signaling, the exit from the systemic circulation of TNF-producing T cells and their entrance into distant lymphoid organs is dependent on the expression of CXCR3 on T cells (61, 62). To determine whether CXCR3 was required for ovx to attract TNF^+ T cells to the BM, SFB^+ *Cxcr3*$^{-/-}$ mice were generated by gavaging SFB^- *Cxcr3*$^{-/-}$ mice purchased from Jackson Laboratory with a liquid suspension of stools from mice previously monocolonized with SFB (43). Ten-week-old female SFB^+ *Cxcr3*$^{-/-}$ mice and WT littermates underwent ovx and were sacrificed 4 weeks later. These experiments were conducted using SFB^+ mice to ascertain whether the recruitment of TNF^+ T cells to the BM is required for the recruitment of Th17 cells to the BM. Ovx increased BM TNF^+ T cells and *Tnf* transcripts in WT, but not in *Cxcr3*$^{-/-}$, mice (Figure 5A). Attesting to the mechanistic role of T cell–produced TNF for CCL20 expression, ovx increased BM *Ccl20* mRNA levels in WT, but it failed to do so in *Cxcr3*$^{-/-}$ mice (Figure 5B). Demonstrating the relevance of the TNF^+ T cells/CCL20 pathway for the homing of Th17 cells to the BM, ovx increased BM Th17 cells, $V\beta14^+$ Th17 cells, and BM *Il17a* transcripts in WT mice, while it did not in *Cxcr3*$^{-/-}$ mice (Figure 5C).

In keeping with the casual role of TNF^+ T cell and Th17 cell homing to the BM for the changes in trabecular bone structure and bone turnover induced by ovx, μCT measurements of femurs and lumbar spines harvested 4 weeks after ovx revealed that ovx decreased BV/TV and altered Tb.Th, Tb.N, and Tb.Sp in WT mice, but not in *Cxcr3*$^{-/-}$ mice (Figure 5, D and E). Moreover, ovx increased serum CTX and osteocalcin levels in WT, but not in *Cxcr3*$^{-/-}$, mice (Figure 5F). However, ovx decreased Ct.Ar and Ct.Th in both *Cxcr3*$^{-/-}$ mice and WT controls (Figure 5G), confirming that ovx caused cortical bone loss through a mechanism unrelated to T cell trafficking. Together, the data were consistent with the hypothesis that the migration of TNF^+ T cells to the BM is required for ovx to induce the homing of intestinal Th17 cells to the BM and the induction of trabecular bone loss.

Discussion

Cytokines produced by BM T cells play a pivotal role in the loss of trabecular bone induced by ovx in mice (5). We report that the TNF^+ T cells and the Th17 cells involved in ovx-induced bone loss originate in the gut and then home to the BM. TNF^+ T cells and Th17 cells egressed the intestine through an S1PR1-dependent mechanism. The influx of TNF^+ T cells into the BM was guided by the chemokine receptor CXCR3. Migration of TNF^+ T cells to the BM and production of TNF by T cells were required for upregulating the expression of the CCR6 ligand CCL20 by BM cells and for the homing of Th17 cells to the BM.

T cell–produced TNF is known to contribute to the bone loss induced by estrogen deprivation in mice (5, 30) and humans (24, 25). However, the origins of BM TNF^+ T cells have not been investigated. This study provided evidence that sex steroid deficiency expanded TNF^+ T cells in the gut and that the increase in BM TNF^+ T cells caused by ovx was secondary to homing of intestinal TNF^+ T cells to the BM. TNF^+ T cells were required to upregulate CCL20 in BM cells and chemoattract Th17 cells to the BM. These findings were consistent with the hypothesis that TNF contributes to ovx-induced bone loss, not only by potentiating the osteoclastogenic activity of RANKL (6, 7), but also by orchestrating the homing of intestinal Th17 cells to the BM.

Th17 cells play a pivotal role in the bone loss resulting from pathologic conditions, such as psoriasis, rheumatoid arthritis, periodontal disease, and inflammatory bowel disease (12, 42). In addition, Th17 cells have been implicated in the bone loss induced by PTH (8, 43) and estrogen deficiency (37–41). While Th17 cells contribute to pathologic bone destruction in autoimmune diseases and bone diseases, the bone erosion induced by Th17 cells serves an important protective role in periodontitis, which is one of the most common infectious diseases, where Th17 cell–induced tooth loss is critical for eradicating bacteria from infected oral cavities and surfaces (63). In addition, IL-17 produced by γδ T cells facilitates fracture repair (64).

Under homeostatic conditions, Th17 cells are most abundant in the gut, where their induction and accumulation are maximized by the presence of SFB in the gut microbiota. Germ-free mice and conventionally raised mice lacking SFB have fewer intestinal Th17 cells and a lower propensity to extraintestinal autoimmune disorders (65, 66); they are protected against the bone loss induced by PTH (43). This suggests a direct functional relationship between microbiota-induced intestinal Th17 cells and Th17-driven tissue injury at peripheral sites.

To directly investigate the effect of ovx on T cell trafficking, we made use of C57BL/6 Kaede mice (52). Kaede mice and similar strains have been successfully used to track the migration of intestinal immune cells, including Th17 cells to the kidney (51), mesenteric lymph nodes (67), and the brain (68). Corroborating information was provided by injecting i.v. EGFP-Th17 cells and measuring their homing to the BM. These experiments revealed that ovx increases the tropism of Th17 cells for the BM in a TNF-dependent fashion.

A mechanistic finding of this study is that the egress of TNF^+ T cells and Th17 cell from the SI was dependent on S1PR1. This insight was obtained using FTY720, a S1PR1 modulator that arrests the exit of all lymphocytes from the intestine to the systemic circulation (58, 59). This drug is currently FDA approved for the treatment of multiple sclerosis. The homing of TNF^+ T cells to the BM was driven by the chemokine receptor CXCR3, which binds to its ligands CXCL9, CXCL10, and CXCL11 (61, 62). These ligands are highly expressed at sites of inflammation as well as constitutively by BM stromal cells and hemopoietic cells (69–71). The influx of Th17 cells into the BM was mediated by the chemokine ligand CCL20, which binds to CCR6. This receptor is expressed by Th17 cells (56, 72). The CCR6/CCL20 axis also drives the recruitment

of intestinal Th17 cells to inflamed kidney (51) and the migration of intestinal Th17 cells to the BM induced by PTH (43).

Earlier studies from our laboratory disclosed that the gut microbiota is required for estrogen deprivation to induce trabecular, but not cortical, bone loss (38). Mechanistically, ovx was found to increase gut permeability, a phenomenon that results in the expansion and activation of TNF^+ T cells and Th17 in the gut and the BM (38). Interestingly, while in conditions of normal gut permeability, the presence of SFB in the gut microbiota is required for Th17 expansion in mice, in mice that had undergone ovx, enhanced gut permeability and the resulting increased translocation of bacteria and bacterial products led to intestinal Th17 expansion even in the presence of SFB negative microbiota. This hypothesis is supported by the finding of the current study and by earlier reports from our laboratory that sex steroid deficiency induces bone loss in conventionally raised mice from Jackson Laboratory, which possess a SFB^- microbiota (33, 35) but not in GF mice, which lack bacterial products translocation (38).

The earlier finding that both intestinal and BM Th17 cells are increased 2 weeks after ovx (38) suggests the possibility that the intestine was the source of the T cells that accumulate in the BM after ovx, but the origin of these cells had remained unknown. The current investigation provided direct evidence that ovx increased gut/BM T cell trafficking. In fact, our data showed that blockade of T cell exit from the gut or blockade of their influx into the BM prevented the expansion of TNF^+ T cells and Th17 cells in the BM, a finding that provided pivotal support to the hypothesis that the T cells implicated in ovx-induced bone loss originate in the gut. Further evidence of the intestinal origin of the Th17 cells involved in ovx-induced bone loss was the finding of the expansion of intestinal-derived $V\beta14^+$ Th17 cells in the BM of mice that had undergone ovx. Attesting to the mechanistic relevance of T cell trafficking, blockade of the egress of TNF^+ T cells and Th17 cells from the gut or their influx into the BM prevented the loss of trabecular bone and the increase in bone turnover induced by ovx. In contrast, cortical bone loss was unrelated to T cell trafficking, a finding consistent with the lack of involvement of the microbiota and T cells in cortical bone loss (38). Direct effects of estrogen on bone cells, including induction of osteoclast apoptosis (3, 4) and inhibition of osteoblast apoptosis (73) are likely to account for the loss of cortical bone induced by ovx. Thus, our results identified the intestine as a proximal target relevant for some of the skeletal effects of ovx.

The findings that ovx increased BM *Tnf* and *Il17a* transcript levels were consistent with the hypothesis that TNF^+ T cells and Th17 are first produced in the gut in response to the microbiota and then homed to the BM, where they contribute to increasing the overall levels of BM TNF and IL-17A. However, we cannot conclusively exclude the possibility that ovx may have also increased the production of TNF and IL-17A by resident BM lineages that were activated by microbial metabolites produced in the gut, which then diffused to the BM (74).

In addition, we cannot entirely discount the possibility that cytokines produced in the gut may have reached the BM via the systemic circulation and contributed to the bone wasting induced by estrogen deficiency. Overall, a major effect of cytokines produced in the intestine is unlikely because, in mice that have undergone ovx, intestinal TNF and IL-17 do not reach concentrations sufficient to exert biological effects at distant anatomical sites. Moreover, the finding that ovx increased BM cytokine transcript levels indicates that cytokines were produced locally.

Although we did not investigate the contribution of intestinal T cell trafficking in other forms of pathologic bone loss, it is likely that a similar mechanism might be relevant for the bone loss induced by inflammatory bowel disease, a condition characterized by increased gut permeability, intestinal T cell activation and expansion, systemic inflammation, and bone loss (75, 76). Intestinal T cell trafficking may also be relevant for the bone loss caused by lactation, which has the purpose of mobilizing calcium from the skeleton. These phenomena are caused by suckling-induced hypogonadotropic hypogonadism, which results in low estrogen levels, and increased secretion of PTH-related peptide (PTHrP) by the breast (77, 78). Since PTH and PTHrP activate the same receptor and induce bone loss by similar mechanisms, Th17 cells are likely to contribute to the skeletal effects of PTHrP. We have reported that PTH promotes the expansion of intestinal Th17 cells and their migration to the BM (43). The current study demonstrates the relevance of Th17 cell trafficking for the bone loss induced by estrogen deficiency. Therefore, homing of intestinal Th17 cells to the BM is likely to be pivotal in lactation-induced skeletal calcium mobilization.

In summary the current study reveals that intestinal T cells are a proximal target of sex steroid deficiency relevant for trabecular bone loss. The observation that blockade of TNF^+ T cells or Th17 cell intestinal egress or blockade of their influx in the BM prevented ovx-induced bone loss provides proof of principle that pharmacological modulation of T cell trafficking may represent a therapeutic strategy for postmenopausal bone loss.

Methods

Mice and in vivo procedures. SFB^+ C57BL/6 mice were purchased from Taconic Biosciences. SFB^- C57BL/6 mice, $Tnf^{-/-}$ mice (B6.129S6-Tnf<tm1Gkl>/J), *Il17a*-EGFP knockin mice (C57BL/6-il17a<tm1Bcgen>/J), $Tcr\beta^{-/-}$ mice (B6.129P2-Tcrb<tm1Mom>/J), and $Cxcr3^{-/-}$ mice (B6.129P2-Cxcr3<tm1Dgen>/J) were purchased from The Jackson Laboratory. Kaede mice (B6.Cg-c/c Tg[CAG-tdKaede]15Utr) were purchased from RIKEN Bioresource Research Center. SFB^+ JAX mice and SFB^+ Kaede mice were generated by oral gavaging SFB^- mice with a liquid suspension of fecal pellets collected from SFB mono-associated mice, as previously described (44). SFB positivity was verified by fecal DNA extraction using the QIAamp DNA Stool Mini Kit (QIAGEN) and subsequent quantitative PCR (qPCR) using an established protocol that used primers that are specific for the SFB 16S rRNA gene: 5′-GACGCTGAGGCATGAGAGCAT-3′, forward; and 5′-GACGGCACGGATTGTTATTCA-3′, reverse; and total bacterial 16S rRNA, 5′-GTGCCAGCMGCCGCGGTAA-3′, forward, and 5′-GGACTACHVGGGTWTCTAAT-3′, reverse. (79). All mice used at Emory University were shipped to the same room in the same vivarium within the Whitehead Biomedical Research Building. All mice were housed under specific pathogen–free conditions and were fed γ-irradiated 5V5R mouse chow (Purina Mills) and autoclaved water ad libitum. The animal facility was kept at 23°C (±1 °C) with 50% relative humidity and a 12-hour light/12-hour dark cycle. All mice were acclimatized within our facility for at least 3 days before experimentation. Sham operation and ovx were performed at the age of 10 weeks using

methods previously established in our laboratory (38, 80, 81). The success of ovx was verified by measuring the uterus weight at sacrifice.

FTY720 treatment. The S1PR1 functional antagonist FTY720 (2-amino-2-[2-(4-octylphenyl) ethylpropane-1,3-diol) was added to the drinking water at 5 μg/mL as described by Krebs et al. (51). FTY720 treatment was initiated 1 day before ovx and continued until sacrifice. Water containing FTY720 was changed weekly.

In vivo anti-CCL20 Ab treatment. Rat anti-CCL20 Ab (clone 114908, R&D Systems, catalog MAB7601) or isotype control (clone 43414, R&D Systems, catalog MAB005) were injected i.p. at 50 μg per mouse 1 day before ovx and every other day thereafter until sacrifice.

Preparation of PP and BM single cell suspension. For PP cell isolation, the SI was removed and flushed of fecal content. PPs were excised and collected in 1 mL cooled RPMI 1640. PPs were dissociated using the plunger of a 2.5 mL syringe and gently forced through a 70 μm cell strainer placed over a 50 mL tube. A single cell suspension was used for flow cytometric analysis. For BM cell isolation, pelvic bones were flushed with PBS and BM cells were collected. RBC lysis was performed twice to eliminate all the red blood cells from BM. Single cell suspension of BM cells was used for analysis by flow cytometry, as previously described (43, 82).

Kaede mice cells photoconversion. Kaede mice express a photoconvertible fluorescence protein that changes from green (518 nm) to red (582 nm) upon exposure to near-UV (350-410 nm) light. Ten-week-old female SFB$^+$ Kaede mice were subjected to sham operation or ovx. Fourteen days after ovx or sham operation, all animals underwent surgical laparotomy, during which the caecum and distal SI were eviscerated and the 4 SI PPs most proximal to the caecum were identified and illuminated with 390 nm wavelength light for 2 minutes each. The caecum and distal SI were reinserted in the abdominal cavity, and the abdominal wall was closed. Aluminum foil was used to protect tissue other than target PPs from light during exposure. Either 24 or 48 hours after photoconversion, mice were sacrificed, and PP cells were collected. A single cell suspension was prepared and analyzed by flow cytometry. BM cells were also collected at sacrifice and single cell suspension prepared. BM KaedeR total T cells were enumerated by flow cytometry by analyzing whole BM cells. Since the number of BM TNF$^+$ T cells and Th17 cells was low, BM cells were enriched for T cells or CD4$^+$ T cells by positive immunomagnetic sorting using mouse CD3ε MicroBeads (Miltenyi Biotec) or mouse CD4 (L3T4) MicroBeads (Miltenyi Biotec). These enriched populations were then utilized for intracellular staining and flow cytometric enumeration of BM TNF$^+$ T cells and Th17 cells.

T cell transfers. *Il17a*-EGFP knockin mice (C57BL/6-IL17atm1 Bcgen/J) express EGFP as a marker of IL-17A activity. Naive CD4$^+$ T cells (CD4$^+$CD44^{lo}CD62L^{hi} cells) were isolated from the spleen of *Il17a*-EGFP mice using the EasySep Mouse Naïve CD4$^+$ T Cell Isolation Kit (STEMCELL Technologies). EGFP$^-$ naive CD4$^+$ T cells were cultured under Th17 polarizing conditions for 4 days using the Mouse Th17 Cell Differentiation Kit (R&D Systems) to generate EGFP$^+$CD4$^+$ Th17 cells. EGFP$^+$CD4$^+$ live Th17 cells were FACS sorted by a FACSAria II (BD Biosciences) and injected (1×10^6 cells per mouse) i.v. into SFB$^-$ JAX WT and *Tnf*$^{-/-}$ recipient mice, which had been subjected to sham operation or ovx 14 days before the T cell transfer. One day after transfer, the relative and absolute frequency of EGFP$^+$CD4$^+$ T cells in the BM of recipient mice was determined by flow cytometry.

WT and *Tnf*$^{-/-}$ spleen T cells were purified by negative immunoselection using the EasySep Mouse T Cell Isolation Kit (STEMCELL Technologies). These cells were injected (5×10^6 cells per mouse) i.v. into *Tcrβ*$^{-/-}$ recipient mice 2 weeks before sham operation or ovx. Successful T cell engraftment was confirmed by flow cytometry of the spleens of the recipient mice harvested at sacrifice.

Flow cytometry. Flow cytometry was performed on a FACSymphony A5 (BD Biosciences), and data were analyzed using FlowJo software (Tree Star). For cell-surface staining, cells were stained with anti-mouse purified CD16/32 (Fc blocking Ab, clone 93, catalog 101302), BV 510-CD45 (clone 30-F11, catalog 103138), BV 421-TCR-β (clone H57-597, catalog 109230), AF 700-CD3 (clone 17A2, catalog 100216), PerCP/Cy5.5-CD4 (clone RM4-5, catalog 100540), BV 711-CD8 (clone 53-6.7, catalog 100748) (BioLegend), BUV395-CD45 (clone 30-F11, catalog 564279), and FITC-Vβ14 T cell receptor (Clone 14-2, catalog 553258) (BD Biosciences). The live cells were discriminated by the Zombie NIR Fixable Viability Kit (BioLegend) or the LIVE/DEAD Fixable Yellow Dead Cell Stain Kit (Thermo Fisher). For intracellular staining, cells were incubated with cell activation cocktail (BioLegend) in the presence of Monensin Solution at 37°C for 12 hours. Anti-mouse PE or APC-IL-17A (clone eBio17B7, catalog 12-717 7-81 or 17-7177-81) (Thermo Fisher) and APC-TNF (clone MP6-XT22, catalog 554420) (BD Biosciences) were added after cell fixation and permeabilization with Intracellular Fixation & Permeabilization Buffer Set (Thermo Fisher).

μCT measurements. μCT scanning and analysis of the distal femur and spine were performed as reported previously (8, 83, 84) using a Scanco μCT 40 scanner (Scanco Medical). Femoral trabecular and cortical bone regions were evaluated using isotropic 12 μm voxels. Spinal trabecular bone was evaluated using isotropic 16 μm voxels. For the femoral trabecular region, we analyzed 70 slices starting 8 slices below the distal growth plate. Femoral cortical bone was assessed using 80 continuous CT slides located at the femoral midshaft. Measurements of spinal trabecular bone contours along the periosteal surfaces were drawn encompassing 50 slices of the L4 vertebra, starting at the beginning of trabecular bone within the spinal body, as described (38). X-ray tube potential was 70 kVp, and integration time was 200 ms. We used the thresholding approach described by Bouxsein et al. (85), which is recommended by Scanco, the mCT-40 manufacturer, and involves a visual inspection and comparison of preview and slice-wise gray-scale 2D images. The same threshold value was used for all measurements.

Bone turnover marker measurement. Serum CTX and osteocalcin were measured by rodent-specific ELISA assays (Immunodiagnostic Systems).

Real-time RT-PCR and primers. Total RNA was isolated using TRIzol reagent (Thermo Fisher Scientific) and the DNase Max Kit (QIAGEN) according to the manufacturer's directions. For all RNA samples, cDNA was synthesized with random hexamer primers (Roche) and AMV reverse transcriptase (Roche). The expression levels of murine *Il17a*, *Tnf*, and *Ccl20* were measured in whole BM cells by real-time PCR. Changes in relative gene expression between sham and ovx groups were calculated using the $2^{-\Delta\Delta CT}$ method with normalization to 18S rRNA. Primer sequences used were as follows: *Il17a*, 5′-TGACGCCCACCTACAACATC-3′, forward, and 5′-CATCATGCAGTTCCGTCAGC-3, reverse; *Tnf*, 5′-AACTCCAGGCGGTGCCTAT-3′, forward, and 5′-TGCCACAAGCAGGAATGAGA-3′, reverse; *Ccl20*, 5′-GCCTCTCGTACATACAGACGC-3′, forward, and 5′-CCAGTTCTGCTTTGGATCAGC-3′, reverse; and 18s rRNA,

5′-ATTCGAACGTCTGCCCTATCA-3′, forward, and 5′-GTCACCCGTGGTCACCATG-3′, reverse.

Statistics. All data are expressed as mean ± SEM. All data were normally distributed according to the Shapiro-Wilk normality test. Data were analyzed by 2-way ANOVA. This analysis included the main effects for animal strain and treatment plus the statistical interaction between animal strain and treatment. When the statistical interaction was statistically significant ($P < 0.05$) or suggestive of an important interaction, then *t* tests were used to compare the differences between the treatment means for each animal strain, applying Bonferroni's correction for multiple comparisons.

Study approval. All animal procedures were approved by the Institutional Animal Care and Use Committee of Emory University in compliance with all applicable federal regulations governing the protection of animals in research.

Author contributions

MNW and RP designed the studies. MY, SP, CWP, JYL, AMT, and JA performed the research and analyzed the animal data. RP, MNW, CMC, and RMJ wrote the manuscript. MY and SP share first authorship because each carried out key experiments of this study. MY appears before SP in the author list because he was the first to work on this project.

Acknowledgments

This study was supported by grants from the NIH (DK112946, DK108842, and RR028009 to RP; AG062334, AR068157, and AR070091 to MNW; GM072808 and GM095442 to CMC). MNW was also supported by a grant from the Biomedical Laboratory Research & Development Service of the VA Office of Research and Development (5I01BX000105). Cameron Paterson acknowledges his funding from United States Navy. The views expressed in this article reflect the results of research conducted by the authors and do not necessarily reflect the official policy or position of the Department of the Navy, Department of Defense, or the US Government. CWP is a military service member or federal/contracted employee of the US government. This work was prepared as part of his official duties. Title 17 USC 105 provides that "copyright protection under this title is not available for any work of the US." Title 17 USC 101 defines a US Government work as work prepared by a military service member or employee of the US Government as part of that person's official duties.

Address correspondence to: Roberto Pacifici, Division of Endocrinology, Metabolism and Lipids, Emory University School of Medicine, 101 Woodruff Circle, Room 1309, Atlanta, Georgia 30322, USA. Phone: 404.712.8420; Email: roberto.pacifici@emory.edu.

1. Khosla S, Pacifici R. In: Marcus R, Feldman D, Dempster DW, Luckey M, Cauley JA eds. *Osteoporosi*s. Amsterdam: Elsvierer; 2013:1113–1138.
2. Weitzmann MN, Pacifici R. Estrogen deficiency and bone loss: an inflammatory tale. *J Clin Invest*. 2006;116(5):1186–1194.
3. Nakamura T, et al. Estrogen prevents bone loss via estrogen receptor alpha and induction of Fas ligand in osteoclasts. *Cell*. 2007;130(5):811–823.
4. Krum SA, et al. Estrogen protects bone by inducing Fas ligand in osteoblasts to regulate osteoclast survival. *EMBO J*. 2008;27(3):535–545.
5. Pacifici R. Role of T cells in ovariectomy induced bone loss-revisited. *J Bone Miner Res*. 2012;27(2):231–239.
6. Cenci S, et al. Estrogen deficiency induces bone loss by enhancing T-cell production of TNF-alpha. *J Clin Invest*. 2000;106(10):1229–1237.
7. Lam J, et al. TNF-alpha induces osteoclastogenesis by direct stimulation of macrophages exposed to permissive levels of RANK ligand. *J Clin Invest*. 2000;106(12):1481–1488.
8. Li JY, et al. IL-17A is increased in humans with primary hyperparathyroidism and mediates PTH-induced bone loss in mice. *Cell Metab*. 2015;22(5):799–810.
9. Chen DY, et al. Increasing levels of circulating Th17 cells and interleukin-17 in rheumatoid arthritis patients with an inadequate response to anti-TNF-α therapy. *Arthritis Res Ther*. 2011;13(4):R126.
10. Sugita S, et al. Inhibition of Th17 differentiation by anti-TNF-alpha therapy in uveitis patients with Behçet's disease. *Arthritis Res Ther*. 2012;14(3):R99.
11. Sato K, et al. Th17 functions as an osteoclastogenic helper T cell subset that links T cell activation and bone destruction. *J Exp Med*. 2006;203(12):2673–2682.
12. Miossec P, et al. Interleukin-17 and type 17 helper T cells. *N Engl J Med*. 2009;361(9):888–898.
13. Basu R, et al. The Th17 family: flexibility follows function. *Immunol Rev*. 2013;252(1):89–103.
14. Komatsu N, Takayanagi H. Autoimmune arthritis: the interface between the immune system and joints. *Adv Immunol*. 2012;115:45–71.
15. Waisman A. T helper cell populations: as flexible as the skin? *Eur J Immunol*. 2011;41(9):2539–2543.
16. Jovanovic DV, et al. IL-17 stimulates the production and expression of proinflammatory cytokines, IL-beta and TNF-alpha, by human macrophages. *J Immunol*. 1998;160(7):3513–3521.
17. Kotake S, et al. IL-17 in synovial fluids from patients with rheumatoid arthritis is a potent stimulator of osteoclastogenesis. *J Clin Invest*. 1999;103(9):1345–1352.
18. Adamopoulos IE, et al. Interleukin-17A upregulates receptor activator of NF-kappaB on osteoclast precursors. *Arthritis Res Ther*. 2010;12(1):R29.
19. Kim YG, et al. IL-17 inhibits osteoblast differentiation and bone regeneration in rat. *Arch Oral Biol*. 2014;59(9):897–905.
20. Uluckan O, et al. Chronic skin inflammation leads to bone loss by IL-17-mediated inhibition of Wnt signaling in osteoblasts. *Sci Transl Med*. 2016;8(330):330ra337.
21. Eghbali-Fatourechi G, et al. Role of RANK ligand in mediating increased bone resorption in early postmenopausal women. *J Clin Invest*. 2003;111(8):1221–1230.
22. Taxel P, et al. Estradiol rapidly inhibits osteoclastogenesis and RANKL expression in bone marrow cultures in postmenopausal women: a pilot study. *Osteoporos Int*. 2008;19(2):193–199.
23. Xiong J, et al. Matrix-embedded cells control osteoclast formation. *Nat Med*. 2011;17(10):1235–1241.
24. D'Amelio P, et al. Estrogen deficiency increases osteoclastogenesis up-regulating T cells activity: a key mechanism in osteoporosis. *Bone*. 2008;43(1):92–100.
25. Adeel S, et al. Bone loss in surgically ovariectomized premenopausal women is associated with T lymphocyte activation and thymic hypertrophy. *J Investig Med*. 2013;61(8):1178–1183.
26. Zhang J, et al. Changes of serum cytokines-related Th1/Th2/Th17 concentration in patients with postmenopausal osteoporosis. *Gynecol Endocrinol*. 2015;31(3):183–190.
27. Pacifici R, et al. Effect of surgical menopause and estrogen replacement on cytokine release from human blood mononuclear cells. *Proc Natl Acad Sci U S A*. 1991;88(12):5134–5138.
28. Cohen-Solal ME, et al. Peripheral monocyte culture supernatants of menopausal women can induce bone resorption: involvement of cytokines. *J Clin Endocrinol Metab*. 1993;77(6):1648–1653.
29. Charatcharoenwitthaya N, et al. Effect of blockade of tumor necrosis factor-alpha and interleukin-1 action on bone resorption in early postmenopausal women. *J Bone Miner Res*. 2007;22(5):724–729.
30. Roggia C, et al. Up-regulation of TNF-producing T cells in the bone marrow: a key mechanism by which estrogen deficiency induces bone loss in vivo. *Proc Natl Acad Sci U S A*. 2001;98(24):13960–13965.
31. Ammann P, et al. Transgenic mice expressing soluble tumor necrosis factor-receptor are protected against bone loss caused by estrogen deficiency.

J Clin Invest. 1997;99(7):1699–1703.
32. Kimble RB, et al. The functional block of TNF but not of IL-6 prevents bone loss in ovariectomized mice. *J Bone Miner Res*. 1997;12(6):935–941.
33. Gao Y, et al. Estrogen prevents bone loss through transforming growth factor beta signaling in T cells. *Proc Natl Acad Sci U S A*. 2004;101(47):16618–16623.
34. Gao Y, et al. IFN-gamma stimulates osteoclast formation and bone loss in vivo via antigen-driven T cell activation. *J Clin Invest*. 2007;117(1):122–132.
35. Li JY, et al. Ovariectomy disregulates osteoblast and osteoclast formation through the T-cell receptor CD40 ligand. *Proc Natl Acad Sci U S A*. 2011;108(2):768–773.
36. Grassi F, et al. Oxidative stress causes bone loss in estrogen-deficient mice through enhanced bone marrow dendritic cell activation. *Proc Natl Acad Sci U S A*. 2007;104(38):15087–15092.
37. Tyagi AM, et al. Estrogen deficiency induces the differentiation of IL-17 secreting Th17 cells: a new candidate in the pathogenesis of osteoporosis. *PLoS One*. 2012;7(9):e44552.
38. Li JY, et al. Sex steroid deficiency-associated bone loss is microbiota dependent and prevented by probiotics. *J Clin Invest*. 2016;126(6):249–2063.
39. Tyagi AM, et al. Enhanced immunoprotective effects by anti-IL-17 antibody translates to improved skeletal parameters under estrogen deficiency compared with anti-RANKL and anti-TNF-α antibodies. *J Bone Miner Res*. 2014;29(9):1981–1992.
40. DeSelm CJ, et al. IL-17 mediates estrogen-deficient osteoporosis in an Act1-dependent manner. *J Cell Biochem*. 2012;113(9):2895–2902.
41. Scheffler JM, et al. Interleukin 17A: a Janus-faced regulator of osteoporosis. *Sci Rep*. 2020;10(1):5692.
42. Martinez GJ, et al. Regulation and function of proinflammatory TH17 cells. *Ann N Y Acad Sci*. 2008;1143:188–211.
43. Yu M, et al. PTH induces bone loss via microbial-dependent expansion of intestinal TNF^+ T cells and Th17 cells. *Nat Commun*. 2020;11(1):468.
44. Ivanov II, et al. Induction of intestinal Th17 cells by segmented filamentous bacteria. *Cell*. 2009;139(3):485–498.
45. Ivanov II, et al. Specific microbiota direct the differentiation of IL-17-producing T-helper cells in the mucosa of the small intestine. *Cell Host Microbe*. 2008;4(4):337–349.
46. Gaboriau-Routhiau V, et al. The key role of segmented filamentous bacteria in the coordinated maturation of gut helper T cell responses. *Immunity*. 2009;31(4):677–689.
47. Atarashi K, et al. Th17 Cell Induction by Adhesion of Microbes to Intestinal Epithelial Cells. *Cell*. 2015;163(2):367–380.
48. Tan TG, et al. Identifying species of symbiont bacteria from the human gut that, alone, can induce intestinal Th17 cells in mice. *Proc Natl Acad Sci U S A*. 2016;113(50):E8141–E8150.
49. Shieh A, et al. Gut permeability, inflammation, and bone density across the menopause transition. *JCI Insight*. 2020;5(2):134092.
50. Bradley CP, et al. Segmented filamentous bacteria provoke lung autoimmunity by inducing gut-lung axis Th17 cells expressing dual TCRs. *Cell Host Microbe*. 2017;22(5):697–704.e4.
51. Krebs CF, et al. Autoimmune renal disease is exacerbated by S1P-receptor-1-dependent intestinal Th17 cell migration to the kidney. *Immunity*. 2016;45(5):1078–1092.
52. Tomura M, et al. Activated regulatory T cells are the major T cell type emigrating from the skin during a cutaneous immune response in mice. *J Clin Invest*. 2010;120(3):883–893.
53. Tomura M, et al. Monitoring cellular movement in vivo with photoconvertible fluorescence protein "Kaede" transgenic mice. *Proc Natl Acad Sci U S A*. 2008;105(31):10871–10876.
54. Yang Y, et al. Focused specificity of intestinal TH17 cells towards commensal bacterial antigens. *Nature*. 2014;510(7503):152–156.
55. Goto Y, et al. Segmented filamentous bacteria antigens presented by intestinal dendritic cells drive mucosal Th17 cell differentiation. *Immunity*. 2014;40(4):594–607.
56. Acosta-Rodriguez EV, et al. Surface phenotype and antigenic specificity of human interleukin 17-producing T helper memory cells. *Nat Immunol*. 2007;8(6):639–646.
57. Baeyens A, et al. Exit Strategies: S1P Signaling and T Cell Migration. *Trends Immunol*. 2015;36(12):778–787.
58. Brinkmann V, et al. FTY720 alters lymphocyte homing and protects allografts without inducing general immunosuppression. *Transplant Proc*. 2001;33(1–2):530–531.
59. Chun J, Hartung HP. Mechanism of action of oral fingolimod (FTY720) in multiple sclerosis. *Clin Neuropharmacol*. 2010;33(2):91–101.
60. Turner JE, et al. CCR6 recruits regulatory T cells and Th17 cells to the kidney in glomerulonephritis. *J Am Soc Nephrol*. 2010;21(6):974–985.
61. Marelli-Berg FM, et al. The highway code of T cell trafficking. *J Pathol*. 2008;214(2):179–189.
62. Groom JR, Luster AD. CXCR3 in T cell function. *Exp Cell Res*. 2011;317(5):620–631.
63. Tsukasaki M, et al. Host defense against oral microbiota by bone-damaging T cells. *Nat Commun*. 2018;9(1):701.
64. Ono T, et al. IL-17-producing γδ T cells enhance bone regeneration. *Nat Commun*. 2016;7:10928.
65. Wu HJ, et al. Gut-residing segmented filamentous bacteria drive autoimmune arthritis via T helper 17 cells. *Immunity*. 2010;32(6):815–827.
66. Lee YK, et al. Proinflammatory T-cell responses to gut microbiota promote experimental autoimmune encephalomyelitis. *Proc Natl Acad Sci U S A*. 2011;108 Suppl 1:4615–4622.
67. Morton AM, et al. Endoscopic photoconversion reveals unexpectedly broad leukocyte trafficking to and from the gut. *Proc Natl Acad Sci U S A*. 2014;111(18):6696–6701.
68. Benakis C, et al. Commensal microbiota affects ischemic stroke outcome by regulating intestinal gammadelta T cells. *Nat Med*. 2016;22(5):516–523.
69. Shin SY, et al. TNFα-exposed bone marrow-derived mesenchymal stem cells promote locomotion of MDA-MB-231 breast cancer cells through transcriptional activation of CXCR3 ligand chemokines. *J Biol Chem*. 2010;285(40):30731–30740.
70. Wuest TR, et al. CXCL10 expressing hematopoietic-derived cells are requisite in defense against HSV-1 infection in the nervous system of CXCL10 deficient mice. *J Neuroimmunol*. 2011;234(1–2):103–108.
71. Yoneyama H, et al. Pivotal role of dendritic cell-derived CXCL10 in the retention of T helper cell 1 lymphocytes in secondary lymph nodes. *J Exp Med*. 2002;195(10):1257–1266.
72. Schutyser E, et al. The CC chemokine CCL20 and its receptor CCR6. *Cytokine Growth Factor Rev*. 2003;14(5):409–426.
73. Yang YH, et al. Estradiol inhibits osteoblast apoptosis via promotion of autophagy through the ER-ERK-mTOR pathway. *Apoptosis*. 2013;18(11):1363–1375.
74. Zaiss MM, et al. The gut-bone axis: how bacterial metabolites bridge the distance. *J Clin Invest*. 2019;129(8):3018–3028.
75. Agrawal M, et al. Bone, inflammation, and inflammatory bowel disease. *Curr Osteoporos Rep*. 2011;9(4):251–257.
76. Collins FL, et al. Immunology of gut-bone signaling. *Adv Exp Med Biol*. 2017;1033:59–94.
77. VanHouten JN, et al. Mammary-specific deletion of parathyroid hormone-related protein preserves bone mass during lactation. *J Clin Invest*. 2003;112(9):1429–1436.
78. Ardeshirpour L, et al. Increased PTHrP and decreased estrogens alter bone turnover but do not reproduce the full effects of lactation on the skeleton. *Endocrinology*. 2010;151(12):5591–5601.
79. Farkas AM, et al. Induction of Th17 cells by segmented filamentous bacteria in the murine intestine. *J Immunol Methods*. 2015;421:104–111.
80. Grassi F, et al. Hydrogen sulfide is a novel regulator of bone formation implicated in the bone loss induced by estrogen deficiency. *J Bone Miner Res*. 2016;31(5):949–963.
81. Li JY, et al. Ovariectomy expands murine short-term hemopoietic stem cell function through T cell expressed CD40L and Wnt10B. *Blood*. 2013;122(14):2346–2357.
82. Li JY, et al. Microbiota dependent production of butyrate is required for the bone anabolic activity of PTH. *J Clin Invest*. 2020;130(4):1767–1781.
83. Robinson JW, et al. T cell-expressed CD40L potentiates the bone anabolic activity of intermittent PTH treatment. *J Bone Miner Res*. 2015;30(4):695–705.
84. Li JY, et al. The sclerostin-independent bone anabolic activity of intermittent PTH treatment is mediated by T-cell-produced Wnt10b. *J Bone Miner Res*. 2014;29(1):43–54.
85. Bouxsein ML, et al. Guidelines for assessment of bone microstructure in rodents using micro-computed tomography. *J Bone Miner Res*. 2010;25(7):1468–1486.